Coking- and Sintering-Resistant Palladium Catalysts Achieved Through Atomic Layer Deposition

Junling Lu, *et al.*

Science **335**, 1205 (2012);
DOI: 10.1126/science.1212906

nodes along $0 < \theta < \pi$ with that for an Enneper's surface with two nodes along $\pi < \theta < 2\pi$. Remarkably, despite the sharp changes in the metric at $\theta = 0$ and π, the sheet does adopt the desired hybrid shape when swelled at room temperature, as shown in Fig. 4 (and as a movie in the SOM). As temperature is increased, Ω_{high} and Ω_{low} both decrease, but also converge, causing the buckled disc to first decrease in size and eventually flatten by 49°C. A subsequent decrease in temperature to 22°C causes the disc to regain its initial shape, although the progression of intermediate shapes is not the same. A more detailed study of the pathways and kinetics of swelling and deswelling is an interesting subject for future study.

In conclusion, we have demonstrated a simple method for halftone lithography of photo-cross-linkable copolymers that permits fabrication of stimulus-responsive gel sheets with micrometer-scale thicknesses and 2D patterned swelling. As long as the dots used to define the halftone pattern are smaller than several times the film thickness, the material behaves as a homogeneous elastic composite on length scales larger than the dot pattern. By patterning spatial variations in dot size, the degree of swelling of the composite gel sheets can be tuned effectively continuously across a wide range using only two high-contrast photomasks. This method provides access not only to simple radially symmetric metrics that yield shapes with nearly constant Gaussian curvature or almost zero mean curvature but also to truly 2D patterns of swelling. Thus, it represents a powerful method for fabricating stimuli-responsive gel micro-devices and studying fundamental questions about how 3D shapes are formed through differential growth in 2D.

References and Notes

1. Z. B. Hu, X. M. Zhang, Y. Li, *Science* **269**, 525 (1995).
2. J. R. Howse *et al.*, *Nano Lett.* **6**, 73 (2006).
3. B. Kaehr, J. B. Shear, *Proc. Natl. Acad. Sci. U.S.A.* **105**, 8850 (2008).
4. G. H. Kwon *et al.*, *Small* **4**, 2148 (2008).
5. E. W. H. Jager, E. Smela, O. Inganäs, *Science* **290**, 1540 (2000).
6. T. Ikeda, M. Nakano, Y. Yu, O. Tsutsumi, A. Kanazawa, *Adv. Mater. (Deerfield Beach Fla.)* **15**, 201 (2003).
7. M. Camacho-Lopez, H. Finkelmann, P. Palffy-Muhoray, M. Shelley, *Nat. Mater.* **3**, 307 (2004).
8. T. J. White *et al.*, *Soft Matter* **4**, 1796 (2008).
9. G. Kofod, W. Wirges, M. Paajanen, S. Bauer, *Appl. Phys. Lett.* **90**, 081916 (2007).
10. A. Lendlein, H. Jiang, O. Jünger, R. Langer, *Nature* **434**, 879 (2005).
11. A. W. Feinberg *et al.*, *Science* **317**, 1366 (2007).
12. P. B. Green, *Int. J. Plant Sci.* **153**, (S3), S59 (1992).
13. U. Nath, B. C. W. Crawford, R. Carpenter, E. Coen, *Science* **299**, 1404 (2003).
14. E. Sharon, M. Marder, H. L. Swinney, *Am. Sci.* **92**, 254 (2004).
15. J. Dervaux, M. Ben Amar, *Phys. Rev. Lett.* **101**, 068101 (2008).
16. H. Liang, L. Mahadevan, *Proc. Natl. Acad. Sci. U.S.A.* **108**, 5516 (2011).
17. Y. Klein, E. Efrati, E. Sharon, *Science* **315**, 1116 (2007).
18. E. Efrati, E. Sharon, R. Kupferman, *Phys. Rev. E Stat. Nonlin. Soft Matter Phys.* **80**, 016602 (2009).
19. M. A. Dias, J. A. Hanna, C. D. Santangelo, *Phys. Rev. E Stat. Nonlin. Soft Matter Phys.* **84**, 036603 (2011).
20. E. Sharon, B. Roman, M. Marder, G.-S. Shin, H. L. Swinney, *Nature* **419**, 579 (2002).
21. E. Sharon, E. Efrati, *Soft Matter* **6**, 5693 (2010).
22. R. Toomey, D. Freidank, J. Rühe, *Macromolecules* **37**, 882 (2004).
23. Z. Cui, J. Du, Y. Gu, *Proc. SPIE* **4984**, 111 (2003).
24. L. Erdmann, A. Deparnay, G. Maschke, M. Längle, R. Brunner, *J. Microlith. Microfab.* **4**, 041601 (2005).
25. M. do Carmo, *Differential Geometry of Curves and Surfaces* (Prentice Hall, New York, 1976).
26. M. M. Müller, M. B. Amar, J. Guven, *Phys. Rev. Lett.* **101**, 156104 (2008).
27. C. S. Peirce, *Am. J. Math.* **2**, 394 (1879).

Acknowledgments: We acknowledge stimulating discussions with M. M. Müller and E. Sharon at the Aspen Center for Physics, where part of this work was done. This research was funded by the Army Research Office through W911NF-11-1-0080 and the National Science Foundation through DMR-0846582, and made use of facilities supported by the NSF Materials Research Science and Engineering Center at the University of Massachusetts (DMR-0747756) and NSF grant BBS-8714235.

Supporting Online Material

www.sciencemag.org/cgi/content/full/335/6073/1201/DC1
Materials and Methods
SOM Text
Figs. S1 to S3
Movie S1
References (*28*–*34*)

14 October 2011; accepted 5 January 2012
10.1126/science.1215309

Coking- and Sintering-Resistant Palladium Catalysts Achieved Through Atomic Layer Deposition

Junling Lu,[1] Baosong Fu,[2] Mayfair C. Kung,[3] Guomin Xiao,[2] Jeffrey W. Elam,[1] Harold H. Kung,[3] Peter C. Stair[4,5]*

We showed that alumina (Al_2O_3) overcoating of supported metal nanoparticles (NPs) effectively reduced deactivation by coking and sintering in high-temperature applications of heterogeneous catalysts. We overcoated palladium NPs with 45 layers of alumina through an atomic layer deposition (ALD) process that alternated exposures of the catalysts to trimethylaluminum and water at 200°C. When these catalysts were used for 1 hour in oxidative dehydrogenation of ethane to ethylene at 650°C, they were found by thermogravimetric analysis to contain less than 6% of the coke formed on the uncoated catalysts. Scanning transmission electron microscopy showed no visible morphology changes after reaction at 675°C for 28 hours. The yield of ethylene was improved on all ALD Al_2O_3 overcoated Pd catalysts.

The two main routes to the deactivation of catalysts consisting of metal nanoparticles (NPs) adsorbed on metal oxide supports are coking (the blocking of the metal surface by the accumulation of carbon on the metal) and sintering (the formation of larger metal particles, which lowers overall surface area and activity). Catalyst deactivation is costly, because catalysts must be regenerated or replaced and because processes are shut down while these steps are taken (*1*). Efforts to solve these two problems have typically focused on one or the other individually, although they often occur simultaneously.

Coke formation (or carbon deposition) during hydrocarbon reactions (*2*–*4*) is often addressed by passivating the active metal with traces of sulfur, triphenylphosphites, tin, bismuth, *et al.* (*5*–*10*); formation of an alloy (*5*, *9*–*12*); or accelerated coke removal through gasification (*9*, *13*). The sintering of metal NPs at high temperatures, particularly above the Tammann temperature (half of the bulk melting point in degrees kelvin), has been prevented in a few cases through steric stabilization by an overlayer of inorganic oxide such as mesoporous silica (*14*, *15*), tin oxide (*16*), zirconia (*17*), or ceria (*18*). In these examples, oxide shells, tens of nanometers thick, are formed around the metal NPs by chemical vapor deposition, dendrimer encapsulation, or grafting. The shell thickness is often poorly controlled, which leads to a decrease in catalytic activity from mass transfer resistance associated with shells that are thicker than desired. None of the above methods has achieved simultaneous inhibition of coking and sintering of supported metal catalysts, while maintaining high catalytic activity in high-temperature applications.

We report that Al_2O_3 overcoats, with a thickness near 8 nm, on supported Pd catalysts can effectively inhibit coke formation and greatly improve the thermal stability of Pd at temperatures

[1]Energy Systems Division, Argonne National Laboratory, Argonne, IL 60439, USA. [2]School of Chemistry and Chemical Engineering, Southeast University, Nanjing, 211189, China. [3]Department of Chemical and Biological Engineering, Northwestern University, Evanston, IL 60208–3120, USA. [4]Department of Chemistry, Northwestern University, Evanston, IL 60208, USA. [5]Chemical Science and Engineering Division, Argonne National Laboratory, Argonne, IL 60439, USA.

*To whom correspondence should be addressed. E-mail: pstair@northwestern.edu

in excess of its Tammann temperature. The Al_2O_3 overcoats were synthesized with precise thickness control by means of atomic layer deposition (ALD) (*19*), a self-limiting growth process for depositing highly conformal thin films on surfaces regardless of whether the materials are flat or possess high-aspect-ratio features, high surface area, or high porosity (*20*–*22*). Surface area measurements [nitrogen isotherm or Brunauer-Emmett-Teller (BET) measurements] and CO chemisorption indicate that the overcoated Pd NPs become accessible to reagent gases through the development of microporosity inside the overcoating layer after high-temperature treatments. When tested for the catalytic oxidative dehydrogenation of ethane (ODHE), which has a documented susceptibility to heavy coke formation at high oxygen conversions (*23*, *24*), the overcoating greatly reduced catalyst deactivation by coking and sintering at high temperatures. In addition, the ethylene yield was increased by more than a factor of 10.

The ALD Al_2O_3 overcoating was carried out in a viscous flow reactor by alternately exposing the sample to cycles of trimethylaluminum and water at 200°C (*19*, *25*). Overcoats with 45 cycles were applied to a conventional Pd/Al_2O_3 catalyst with a particle size of 2.8 ± 0.52 nm ($45Al/Pd/Al_2O_3$), synthesized by wet impregnation onto γ-Al_2O_3. The overcoat thickness was 7.7 ± 0.4 nm, according to high-resolution transmission electron microscope measurements [figs. S1 and S2 (*19*)]. The Pd loadings before and after overcoating, as determined by inductively coupled plasma atomic emission spectroscopy, were 1.88 and 1.03%, respectively.

ODHE was conducted using a feed stream containing ethane and oxygen at a ratio of 3:1. The activities of the catalyst with and without ALD Al_2O_3 overcoating were compared by using the same weight of metal in the reactor. The reaction tests were conducted in a quartz tube reactor, with the void space packed with fine quartz chips to suppress homogeneous gas-phase reactions. The catalyst, diluted with 1 g of fine quartz chips, was heated in a stream of 10% oxygen in helium at a ramp rate of 2°C/min to 700°C and held at that temperature for 120 min before the ODHE reaction test. The flow rates of ethane, oxygen, and helium were 9, 3, and 38 standard cubic centimeters per minute (sccm), respectively (*19*).

At 675°C, the initial ethane and oxygen conversions were 55 and 100%, respectively, for the uncoated Pd/Al_2O_3 sample after being stabilized for 10 min. This catalyst demonstrated a very poor performance (Fig. 1); the major products were CO and CO_2, at a yield of 12 and 6%, respectively, whereas the yield of the desired product, ethylene, was only 1.9%. All product yields quickly decreased to zero in less than 30 min when the reactor was completely plugged by coke and the reaction stopped, consistent with previous reports (*23*, *24*).

The Pd sample overcoated with 45 cycles of ALD Al_2O_3 demonstrated some decrease in activity: Ethane and oxygen conversions were 37 and 99% at a steady state, respectively. However, this catalyst showed dramatic improvements in performance, with an increased yield of ethylene and stable activity for ~1700 min [Fig. 1 and fig. S3 (*19*)]. The yield of ethylene, which was initially 12% and then gradually increased to a steady state of 23% after about 500 min, is competitive with the best catalysts for ODHE reported (*26*–*29*). The yields of undesired products—CO, CO_2, and CH_4—were suppressed and were stable at 5.1, 3.9, and 0.9%, respectively. The increased yield of CO relative to CO_2 most likely results from the reverse water gas shift (WGS) reaction and from CO_2- and H_2O-facilitated dehydrogenation in this oxygen-depleted environment (*26*, *30*).

We quantified the reduced coke formation by the ALD Al_2O_3 overcoat using in situ thermogravimetric analysis under reaction conditions with a flow of ethane (10.5 sccm), oxygen (3.5 sccm), and helium (66.5 sccm) over the catalyst at 650°C. For the uncoated Pd/Al_2O_3 sample, 11.83 mg of coke was formed on 20 mg of sample after 60 min of reaction. For $45Al/Pd/Al_2O_3$, the deposited coke was reduced by 94% to only 0.40 mg [fig. S4 (*19*)]. Inhibition of coke formation on $45Al/Pd/Al_2O_3$ as compared with the

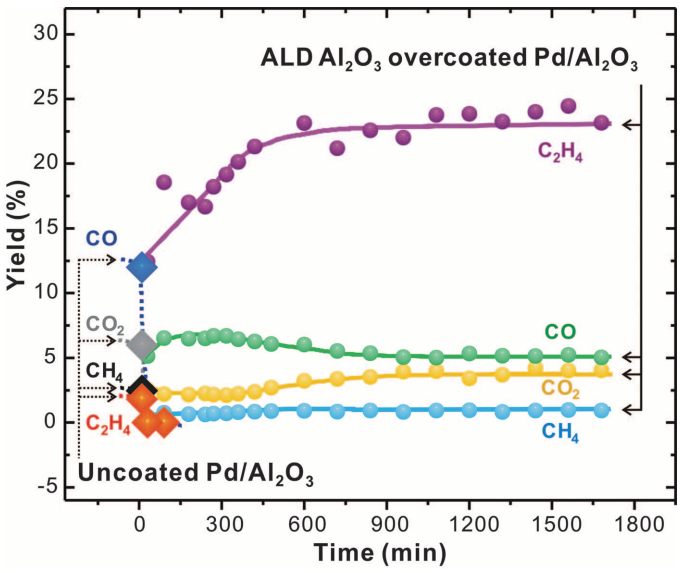

Fig. 1. Products yield on the Pd/Al_2O_3 samples with and without ALD Al_2O_3 overcoat during ODHE reaction as a function of reaction time under identical reaction conditions. Diamonds with a dashed line, product yields on the uncoated Pd/Al_2O_3 sample; circles with solid lines, product yields on the $45Al/Pd/Al_2O_3$ sample.

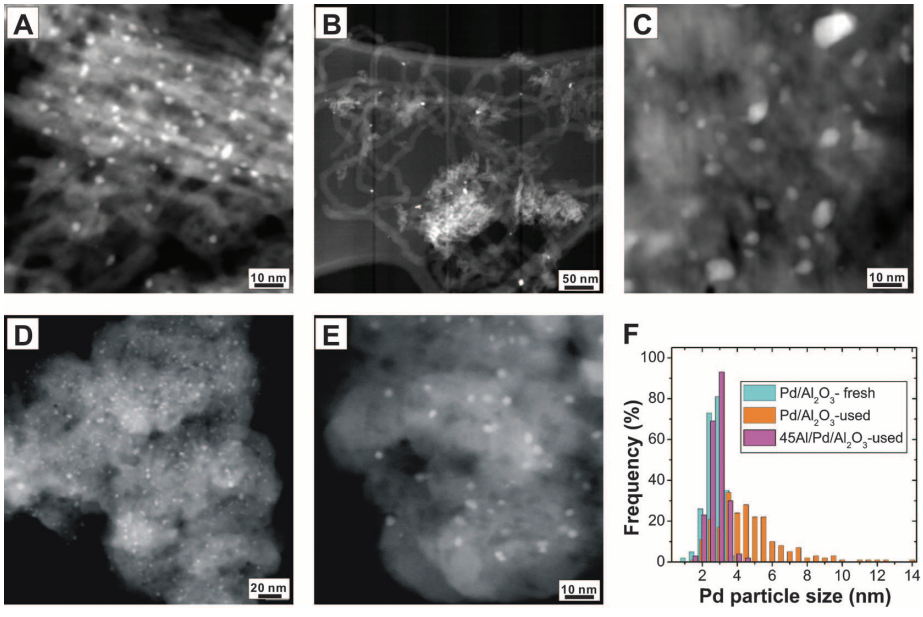

Fig. 2. STEM images of fresh and used samples after ODHE reaction testing. (**A**) The fresh Pd/Al_2O_3 sample. (**B** and **C**) The used Pd/Al_2O_3 sample at 675°C for 30 min at low (B) and high (C) magnification. (**D** and **E**) The used $45Al/Pd/Al_2O_3$ sample at 675°C for ~1700 min at low (D) and high (E) magnification. (**F**) Pd particle size distributions of these three samples.

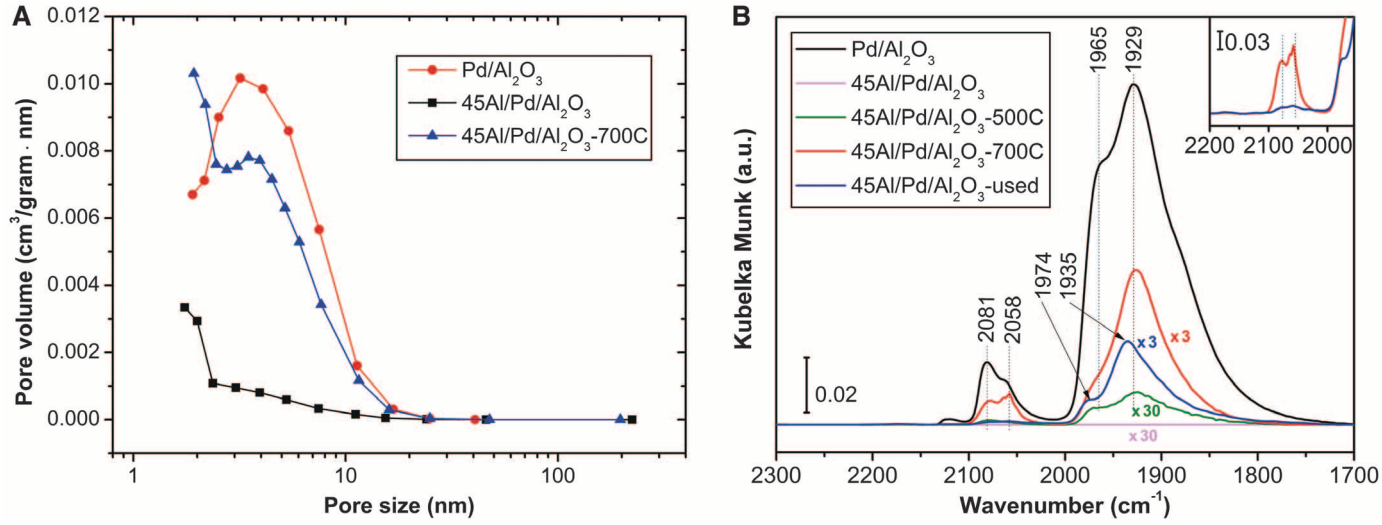

Fig. 3. Structural characterization of ALD Al_2O_3 overcoats and accessibility of embedded Pd NPs after high-temperature treatments. (**A**) Pore size distribution calculated from the adsorption branch of BET isotherms: the uncoated Pd/Al_2O_3, fresh $45Al/Pd/Al_2O_3$, and $45Al/Pd/Al_2O_3$-700C samples. (**B**) IR spectra of CO chemisorption on the Pd samples with and without ALD Al_2O_3 overcoats at the CO saturation coverage: the uncoated Pd/Al_2O_3, fresh $45Al/Pd/Al_2O_3$, $45Al/Pd/Al_2O_3$-500C, $45Al/Pd/Al_2O_3$-700C, and $45Al/Pd/Al_2O_3$-used samples. IR absorbance is in arbitrary Kubelka-Munk units. The inset is the higher–wave number region for the $45Al/Pd/Al_2O_3$-700C and $45Al/Pd/Al_2O_3$-used samples, showing the near-absence of edge and corner sites after reaction.

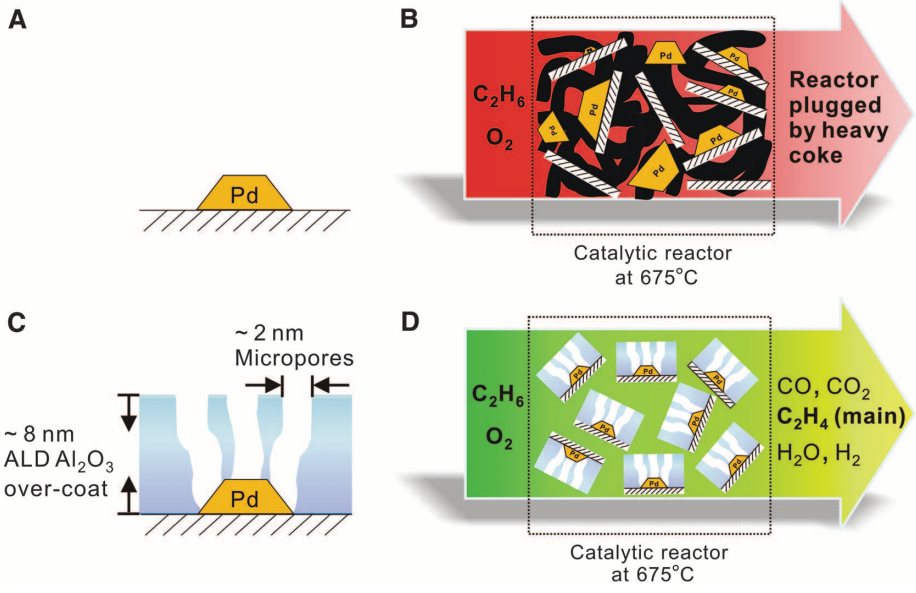

Fig. 4. A schematic model of Pd/Al_2O_3 catalysts with and without ALD Al_2O_3 overcoat during ODHE reaction at 675°C. (**A**) The uncoated Pd/Al_2O_3 catalyst. (**B**) The uncoated Pd/Al_2O_3 catalyst during ODHE reaction, in which filamentous carbon (thick black lines) plugged the reactor and there was substantial sintering and leaching of Pd NPs from the support (barred white lines). (**C**) The Pd catalyst with an ~8-nm ALD Al_2O_3 overcoat, which contained ~2-nm micropores after activation. (**D**) The ALD Al_2O_3–overcoated Pd/Al_2O_3 catalyst during ODHE reaction, on which the microporous Al_2O_3 overcoat trapped and stabilized the Pd NPs, inhibiting Pd NP leaching and coke formation, while greatly enhancing ethylene formation.

uncoated catalyst explains the maintenance of high activity at 675°C in Fig. 1.

The effect of overcoating on the thermal stability of Pd particles was determined from particle size measurements in fresh and used catalysts, using scanning TEM [(STEM), with a JEOL JEM-2100F microscope]. For the used uncoated Pd/Al_2O_3 catalyst, a large amount of filamentous carbon was observed, consistent with coke formation during the ODHE reaction (Fig. 2B). Leaching of Pd NPs from the Al_2O_3 support driven by filamentous carbon growth was also observed (Fig. 2B) (*2*–*4*). After only 30 min of reaction at 675°C, the Pd NPs also became substantially larger, with a much broader particle size distribution due to sintering (4.6 ± 1.92 nm, Fig. 2, B, C, and F). However, the Pd particle size on the $45Al/Pd/Al_2O_3$-used catalyst (2.8 ± 0.46 nm, Fig. 2, D to F) was essentially unchanged after ~1700 min of reaction at 675°C. We determined that 45 cycles of ALD Al_2O_3 were required to stabilize Pd NPs under these high-temperature reaction conditions, because some sintering was observed after reaction on a catalyst coated with only 30 cycles of ALD Al_2O_3 [figs. S9 to S11 (*19*)].

The porosity of the ALD Al_2O_3 overcoats after high-temperature pretreatment was determined by nitrogen BET measurements (with an ASAP 2020 analyzer, Micromeritics). In order to measure the changes in surface area and pore size distribution, the quantity of adsorbed nitrogen and the surface area were normalized based on the weight of the starting catalyst, Pd/Al_2O_3. The BET surface area decreased from 253 to 30 m^2/gram on the freshly coated material [figs. S5 and S6 (*19*)]. Calcining at 700°C for 120 min in 10% oxygen in helium, followed by reduction in 5% hydrogen in helium at 300°C for 30 min ($45Al/Pd/Al_2O_3$-700C), restored the BET surface area to 213 m^2/gram [fig. S7 (*19*)]. Figure 3A shows that the initial, uncoated Pd/Al_2O_3 catalyst was mesoporous, with an average pore size of 6.6 nm. After 45 cycles of ALD Al_2O_3 overcoating, the mesopores disappeared, revealing the dramatic BET surface area decrease. This result is not surprising, because the thickness of the ALD Al_2O_3 overcoat was sufficient to fill the mesopores. After high-temperature treatment, 6.6-nm mesopores reappeared, and new, ~2-nm pores were formed (Fig. 3A). The pores formed as a result of structural changes in the amorphous Al_2O_3 overcoating layer caused by dehydration (*31*), the removal of carbon residues

resulting from the ALD process, and dewetting of the Al_2O_3 overcoats from the surface of the Pd NPs. The latter may be the result of the large lattice mismatch between palladium and alumina. These pores made it possible for the embedded Pd NPs to be accessible to reagents, while the overcoat imparted high thermal stability.

To further determine the accessibility of the Pd NPs embedded under the ~8-nm-thick ALD Al_2O_3 overcoat, we measured diffuse reflectance infrared (IR) spectra using CO as a probe molecule, because there is extensive information about CO chemisorption on Pd NPs (*19*, *32*). As shown in Fig. 3B, the fresh Pd/Al_2O_3 sample without an Al_2O_3 overcoat exhibited two strong peaks at 1929 and 1965 cm^{-1} and two weaker peaks at 2058 and 2081 cm^{-1}. These peaks can be assigned to μ_2-bridge-bonded CO on (111) facets, μ_2-bridge-bonded CO on step and facet edges, linear CO on step and facet edges, and linear CO on the Pd corner atoms of Pd NPs, respectively (*25*, *32*). After 45 cycles of ALD Al_2O_3 were applied, all of the CO chemisorption peaks disappeared, which is consistent with complete covering of the Pd NPs. However, after calcination at 500°C for 120 min in 10% oxygen in helium and then reduction in 5% hydrogen in helium at 300°C for 30 min ($45Al/Pd/Al_2O_3$-500C), a low-intensity chemisorbed CO peak was detected. The restored chemisorbed CO peak became more pronounced when the calcination temperature was increased to 700°C, followed by the same reduction procedure ($45Al/Pd/Al_2O_3$-700C). These results clearly indicated that the ALD Al_2O_3 overcoats became porous after high-temperature treatments, restoring gas accessibility to the Pd NPs, which is consistent with the BET measurements. On the used sample ($45Al/Pd/Al_2O_3$-used), the bridge-bonded CO IR feature is very similar to that of the $45Al/Pd/Al_2O_3$-700C sample, except for a slight decrease in intensity and a small blue shift due to CO-CO lateral interactions. In comparison to uncoated Pd NPs, the features associated with CO bonded to edges and corners on the coated samples had substantially lower intensity than the feature due to CO on facet planes, which indicates that the Al_2O_3 overcoating preferentially decorated the low-coordinated Pd sites, such as steps and edges on both the 700°C activated and used samples.

Figure 4 shows a schematic model of Pd/Al_2O_3 catalysts with and without an ALD Al_2O_3 overcoat during ODHE reaction at 675°C. For the uncoated Pd/Al_2O_3 catalyst, substantial deactivation of Pd was due to heavy coking by filamentous carbon and Pd particle sintering, with leaching of Pd from the Al_2O_3 support surface (Fig. 4, A and B). For the ALD Al_2O_3–overcoated Pd/Al_2O_3 catalyst, the ALD Al_2O_3 overcoat preferentially blocks the low-coordinated Pd surface sites that favor C-C bond scission and hydrogen stripping to produce C1 fragments that lead to coke, CH_4, CO, and CO_2 while favoring the formation of ethylene on the facets (*12*, *33*). The role of C1 species in coking is supported by the observation that when the hydrocarbon reagent was methane, coke was formed on the alumina-overcoated Pd catalysts, but not when either ethane or propane was the reagent [figs. S15 and S16 and table S1 (*19*)]. The identification of low-coordinated Pd surface sites as the centers for coke formation is consistent with Nørskov *et al*., who observed that carbon nanofibers developed initially at step edges on nickel surfaces (*34*). They also found that restructuring of atomic step edges on the nickel surface, a process that involves surface diffusion of both carbon and nickel atoms, facilitated fiber growth. Because Ostwald ripening also proceeds via the release of low-coordinated surface metal atoms, the edge and corner atoms play a central role in both sintering and coking (*34*). Therefore, exceptional resistance to sintering and coking in high-temperature catalytic reactions appears to be achieved because the edge and corner atoms are selectively blocked and stabilized by alumina overcoats. Meanwhile, a lower selectivity to ethylene on alumina-coated catalysts with a smaller particle size is expected and was observed [table S2 (*19*)], because the terraces are a smaller portion of the surface on the smaller particles.

Additional contributions to coke inhibition that are consistent with the model of Fig. 4 cannot be ruled out. (i) The Al_2O_3 overcoat divides the Pd NPs' surface into ensembles of Pd atoms that are too small to support coke formation. This follows a model proposed by Sachtler *et al*., in which hydrogenolysis reactions require large ensembles, whereas the adsorption of modifiers (sulfur, gold, tin, and carbon) breaks up the periodicity of the surface to prevent coke formation (*10*). (ii) The size of the pore channels in the alumina overcoat inhibits carbon filament formation, because the typical filament diameter is much larger (~17 nm) than the pore diameter in the Al_2O_3 overcoat (Figs. 2B and 3A). (iii) The concentrations of reagents, including reactants and products, are limited within the microporous channels at the Pd NPs, so that bimolecular reactions (including radical chains) that are necessary to form coke are inhibited.

Finally, in order to determine the contribution to ethylene selectivity from nonoxidative DHE, the reaction in the absence of oxygen was examined on another 45-cycle ALD Al_2O_3–coated Pd sample under otherwise identical conditions. The yield of ethylene was only 4.6% at the ethane conversion of 7.0% [fig. S17 (*19*)]. Ethylene formed through the direct DHE reaction pathway contributed only a minor amount to the dramatic increase in ethylene yield observed for the ODHE reaction. Most likely, CO_2- and H_2O-facilitated dehydrogenation play an important role toward the end of the catalyst bed, where oxygen has been consumed (*19*, *26*, *30*).

References and Notes

1. R. J. Farrauto, C. H. Bartholomew, *Fundamentals of Industrial Catalytic Processes* (Blackie, London, 1997).
2. J. Barbier, *Appl. Catal.* **23**, 225 (1986).
3. J. A. Moulijn, A. E. van Diepen, F. Kapteijn, *Appl. Catal. A Gen.* **212**, 3 (2001).
4. E. E. Wolf, F. Alfani, *Catal. Rev.* **24**, 329 (1982).
5. J. R. Rostrup-Nielsen, I. Alstrup, *Catal. Today* **53**, 311 (1999).
6. K. K. Ghosh, D. Kunzru, *Ind. Eng. Chem. Res.* **27**, 559 (1988).
7. D. T. Wickham, J. Engel, M. E. Karpuk, U.S. Patent 6,482,311 B1 (2002).
8. J. Radnik *et al*., *Angew. Chem. Int. Ed.* **44**, 6771 (2005).
9. D. L. Trimm, *Catal. Today* **49**, 3 (1999).
10. P. Biloen, J. N. Helle, H. Verbeek, F. M. Dautzenberg, W. M. H. Sachtler, *J. Catal.* **63**, 112 (1980).
11. N. Macleod, J. R. Fryer, D. Stirling, G. Webb, *Catal. Today* **46**, 37 (1998).
12. A. K. Rovik, S. K. Klitgaard, S. Dahl, C. H. Christensen, I. Chorkendorff, *Appl. Catal. A Gen.* **358**, 269 (2009).
13. T. Horiuchi *et al*., *Appl. Catal. A Gen.* **144**, 111 (1996).
14. S. H. Joo *et al*., *Nat. Mater.* **8**, 126 (2009).
15. M. Seipenbusch, A. Binder, *J. Phys. Chem. C* **113**, 20606 (2009).
16. K. Yu, Z. C. Wu, Q. R. Zhao, B. X. Li, Y. Xie, *J. Phys. Chem. C* **112**, 2244 (2008).
17. P. M. Arnal, M. Comotti, F. Schuth, *Angew. Chem. Int. Ed.* **45**, 8224 (2006).
18. M. Cargnello *et al*., *Dalton Trans.* **39**, 2122 (2010).
19. Materials, methods, and supporting data are available on *Science* Online.
20. S. M. George, *Chem. Rev.* **110**, 111 (2010).
21. R. L. Puurunen, *J. Appl. Phys.* **97**, 121301 (2005).
22. B. S. Lim, A. Rahtu, R. G. Gordon, *Nat. Mater.* **2**, 749 (2003).
23. M. Huff, L. D. Schmidt, *J. Phys. Chem.* **97**, 11815 (1993).
24. S. S. Bharadwaj, L. D. Schmidt, *J. Catal.* **155**, 403 (1995).
25. H. Feng, J. L. Lu, P. C. Stair, J. W. Elam, *Catal. Lett.* **141**, 512 (2011).
26. F. Cavani, N. Ballarini, A. Cericola, *Catal. Today* **127**, 113 (2007).
27. P. Concepcion *et al*., *Catal. Today* **96**, 179 (2004).
28. Z. S. Chao, E. Ruckenstein, *J. Catal.* **222**, 17 (2004).
29. K. D. Chen, A. T. Bell, E. Iglesia, *J. Phys. Chem. B* **104**, 1292 (2000).
30. K. Nakagawa *et al*., *Catal. Today* **84**, 149 (2003).
31. J. D. Ferguson, A. W. Weimer, S. M. George, *Thin Solid Films* **371**, 95 (2000).
32. T. Lear *et al*., *J. Chem. Phys.* **123**, 174706 (2005).
33. Z. P. Liu, P. Hu, *J. Am. Chem. Soc.* **125**, 1958 (2003).
34. S. Helveg *et al*., *Nature* **427**, 426 (2004).

Acknowledgments: The work was financially supported by The Dow Chemical Company under the Dow Methane Challenge Award and by the U.S. Department of Energy, Office of Basic Energy Sciences, Hydrogen Fuel Initiative, Chemical Sciences, under contract DE-AC-02-06CH11357. Applications for U.S. and international patents with the title "Metal Catlayst Composition" have been filed. All data and images are available in the body of the paper or as supporting online material. We thank J. T. Miller for providing the Pd/Al_2O_3 sample, F. A. Rabuffetti and K. R. Poeppelmeier for technical assistance on TGA measurements, M. M. Schwartz and C. L. Marshall for technical assistance on BET measurements, F. H. Ribeiro and F. Sollberger for particle dispersion measurements, and N. M. Schweitzer and D. Barton for helpful discussions. B.F. acknowledges financial support in part by the China Scholarship Council.

Supporting Online Material

www.sciencemag.org/cgi/content/full/335/6073/1205/DC1
Materials and Methods
Figs. S1 to S17
Tables S1 and S2
References (*35*–*41*)

19 August 2011; accepted 2 February 2012
10.1126/science.1212906